Breakthrough spectrophotometric instrument for the ultra-fine characterization of the spectral transmittance of thin-film optical filters

Michel Lequime, Myriam Zerrad, Claude Amra

Research Article | Vol. 26, No. 26 | 24 Dec 2018 | OPTICS EXPRESS 34236
Optics EXPRESS

Breakthrough spectrophotometric instrument for the ultra-fine characterization of the spectral transmittance of thin-film optical filters

MICHEL LEQUIME,* MYRIAM ZERRAD, AND CLAUDE AMRA

Aix Marseille Univ, CNRS, Centrale Marseille, Institut Fresnel, Marseille, France
*michel.lequime@fresnel.fr

Abstract: In this paper, we provide a detailed description of the main features of the upgraded version of a spectrophotometric apparatus developed by our team since 2014 [Opt. Express **23**, 26863 (2015)]), and whose improved performance allows the characterization over the visible and near infrared part of the spectrum of the transmittance of complex interference filters with high spectral resolution (approximately one tenth of a nanometer) and an extremely wide dynamic range (thirteen decades).

1. Introduction

Since the end of the 1990s, the simultaneous availability of powerful optical filter design software [1–4] and reliable thin-film deposition techniques using energetic processes [5–7] such as ion beam assistance, ion beam sputtering or magnetron sputtering have made possible the manufacture of high performance optical interference coatings comprising a great number of layers, from one hundred [8] up to a few thousand [9, 10]. For highly demanding applications such as observation of the Earth from space [11, 12], wavelength multiplexing of high data rate optical telecommunications channels [13, 14], study of the organization of living matter at the cellular scale [15], or interferometric detection of gravitational waves [16, 17], it is necessary to confirm by very accurate measurements the theoretical figures provided by the design, especially for some key filter parameters like optical density in the blocking regions, steepness of band edges, or wavelength and angle resolved scattering.

Recently [18, 19], we demonstrated the ability of a spectrophotometric apparatus, based on the combined use of a high-power super-continuum laser source, a tunable volume hologram filter, a standard Czerny-Turner monochromator and a scientific grade CCD camera, to record the transmittance of a thin-film filter over an ultra-wide range of optical densities (from 0 to 11) between 400 and 1000 nm. In this set-up, the CCD camera was only used as a low-noise integrating detector, the final stage of spectral filtering being ensured by a 200 μm diameter circular core fiber whose input end was located at the output port of the spectrograph, equipped with a 300 lines/mm ruled grating, and with output end imaged with a magnification of approximately 2.3 at the surface of this CCD camera.

To improve the performance of this set-up with regard to resolution, versatility, and robustness to light interference, some changes were made to the reference channel and detection sub-assemblies so as to simultaneously record at high resolution (typically 0.1 nm) the spectra of the incoming and transmitted light fluxes. To this end we fitted the turret of our spectrograph with a high dispersion holographic grating and installed on the output port a scientific grade CCD camera with shape and pixel size adapted to the recording of a spectrally dispersed signal; as the input slit we used a customized 2-leg fiber bundle, with one leg linked to the optical receiver assembly used for our transmittance or scattering measurements and the other directly connected to the reference arm.

This article gives a detailed presentation of this improved apparatus, including a description of

#349787 https://doi.org/10.1364/OE.26.034236
Journal © 2018 Received 31 Oct 2018; revised 11 Dec 2018; accepted 11 Dec 2018; published 17 Dec 2018

Optics EXPRESS

the method developed for processing the recorded data, and an illustration of the performance of this set-up in various cases (spectral transmittance properties of band-pass and edge filters, spectral transmittance of silver layers with thicknesses from a few nanometers to several hundred nanometers).

2. Materials and Methods

2.1. Spectrophotometric apparatus

A schematic representation of the improved version of our set-up is given in Fig. 1.

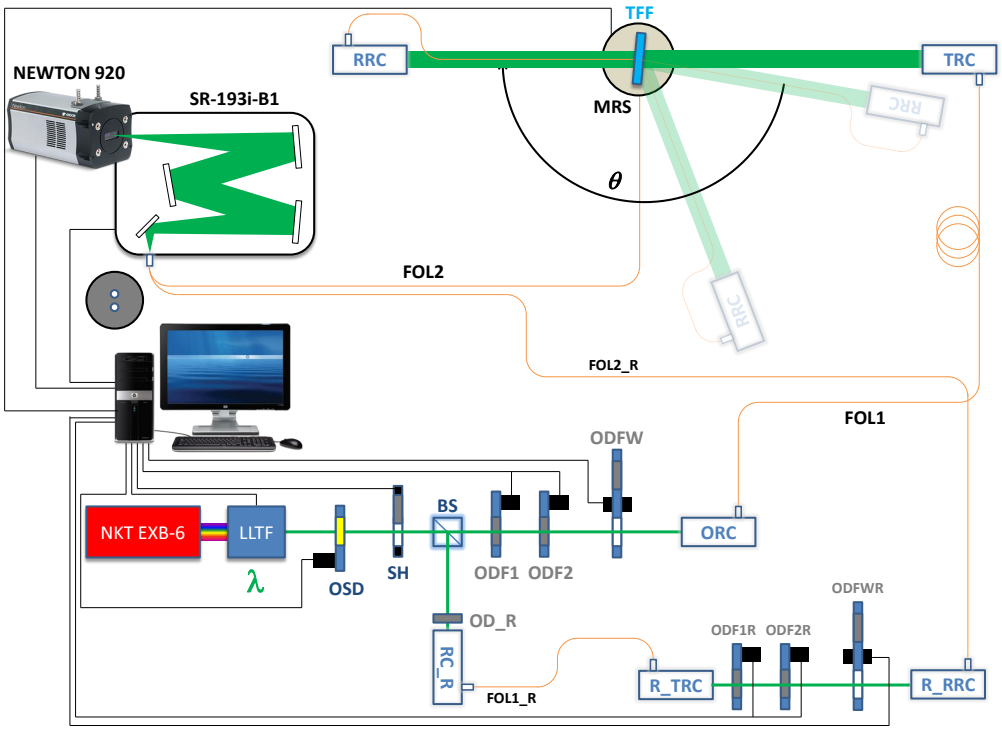

Fig. 1. Schematic representation of the improved performance spectrophotometric apparatus (NKT EXB-6: super-continuum laser source; LLTF: tunable volume hologram filter; OSD: order sorting device; SH: shutter; BS: beam splitter; ODF1: optical density flip 1; ODF2: optical density flip 2; ODFW: optical density filter wheel; ORC: output reflective collimator; FOL1: fiber optic link 1; TRC: transmitter reflective collimator; TFF: thin-film filter; MRS: motorized rotating stage; RRC: receiving reflective collimator; FOL2: fiber optic link 2; SR-193i-B1: motorized Czerny-Turner monochromator; NEWTON 920: scientific grade CCD camera; OD R: reference optical density; RC R: reference reflective collimator; FOL1 R: reference fiber optic link 1; R_TRC: reference transmitter reflective collimator; ODF1R: reference optical density flip 1; ODF2R: reference optical density flip 2; ODFWR: reference optical density filter wheel; R_RRC: reference receiving reflective collimator; FOL2_R: reference fiber optic link 2).

A low divergence quasi-monochromatic light beam with a mean power around 1 mW, a central wavelength tunable between 400 and 1000 nm, and a bandwidth of approximately 2 nm is obtained through the spectral filtering of a 6 Watts supercontinuum laser source (NKT Photonics) by a volume Bragg grating (Laser Line Tunable Filter Contrast VIS from PHOTON Etc). An

Optics EXPRESS

order sorting device (OSD) consisting of two edge filters installed in a flip mount is used for removing the parasitic harmonic lines that result firstly from non-linearities in the refractive index modulation within the volume of the hologram and secondly from the higher orders of the interference filtering function [18]. An electro-mechanical shutter SH is inserted into the beam (in the closed position by default) to define the effective integration time of the measurement performed for each central wavelength selected by the tunable filter. A non-polarizing beam splitter (BS) reflects a small portion (typically 10%) of the incoming beam toward a reference channel while the main beam passes through three stages of reflective optical densities [19]. The first two (ODF1 and ODF2, each with an optical density of approximately 3) are installed in two-position, high-speed 0-90 degree flip mounts, while the third (ODFW) is mounted on a 6-slot motorized fast change filter wheel (slot 1: no optical density; slot 2: OD 1; slot 3: OD 2; slot 4: OD 3; slots 5 and 6 not used). All these mechanical devices are remotely operated, so that at any time we can alter the value of the optical density in the measurement arm between zero and nine in steps of one [19]. The attenuated beam is then focused by a silver-coated, off-axis, parabolic mirror (ORC, output reflective collimator) onto the 2a = 50 μm diameter core of a step-index all silica fiber (FOL1, fiber optic link 1). The output end of this FOL1 fiber is connected to the focal plane of an aspherical mirror (TRC, transmitter reflective collimator) that delivers a collimated, aberration-free beam passing through the thin-film filter (TFF) whose optical properties have to be measured. The light flux transmitted, reflected or scattered by this filter in a small solid angle dΩ around θ is focused by the same type of optical element (RRC, receiving reflective collimator) onto the input end of a 2a = 100 μm diameter core of a step-index all silica fiber (FOL2, fiber optic link 2).

The beam reflected by the non-polarizing beam splitter BS is attenuated by an optical density OD_R before being focused by a parabolic off-axis reflective collimator (RC_R) onto the 2a = 50 μm diameter core of a step-index all silica fiber (FOL1_R, reference fiber optic link). The output end of this reference fiber is connected to the focal plane of an off-axis parabolic mirror (R_TRC, reference transmitter reflective collimator) that delivers a collimated beam passing through three stages of reflective optical densities; implementation is similar to that used on the main beam, but with different levels of attenuation: OD 1.6 on the ODF1R flip, OD 3.3 on the ODF2R flip and the following sequence (slot 1: metallic stop corresponding to an infinite OD; slot 2: no density; slot 3: OD 0.3; slot 4: OD 0.6; slot 5: OD 1.0; slot 6: OD 1.3) on the ODFWR filter-wheel. The remote operability of these three devices allows us to select a value for the optical density in the reference arm of between zero and approximately 6 in steps of 0.3. The reference attenuated beam is focused by a reflective collimator (R_RRC, reference receiving reflective collimator) onto the input end of a 2a = 100 μm diameter core of a step-index all silica fiber (FOL2_R, reference fiber optic link 2).

The output ends of both fiber optic links (FOL2 and FOL2_R) are mounted in a common metal ferrule (distance between fiber cores of 3.1 mm) and connected to the input port of an ANDOR Czerny-Turner monochromator (reference SHAMROCK SR-193i-B1). A holographic grating with 1800 lines per millimeter is located on the motorized turret of this spectrograph and its angular position can be remotely controlled through a USB 2.0 link. The output port of this monochromator is equipped with a scientific grade back-illuminated visible-optimized anti-fringing CCD camera, again from ANDOR (reference NEWTON DU920P-BVF), using 255 x 1024 square pixels, each of 26 μm. The lateral magnification of the spectrograph is equal to 1.07, while its spatial dispersion D has been measured to 0.04778 nm/pixel around 633 nm. Hence the spectral bandwidth covered by a CCD line is approximately ±25 nm around the central wavelength defined by the turret angular position, with a sampling pitch of about 0.05 nm; the vertical distance between the centers of the fiber core images is about 127 pixels for a core image diameter of approximately 4 pixels.

Optics EXPRESS

2.2. Principle of operation

For instance, to measure the spectral transmittance of a thin-film filter at a wavelength λ we chose (as previously defined [18, 19]) to replace a direct comparison between the powers of the incoming and transmitted light by the locking of the maximum signal provided by the CCD camera onto a high and approximately constant level equal to 70% ± 10% of its full well capacity (FWC), i.e. to 50,000 ± 7,500 in terms of the digitized signal.

Let us consider first the MES spectrum associated with the spatial dispersion of the slightly polychromatic light emitted from the end of the FOL2 fiber. The locking of its maximum signal is achieved through the combined adjustment of two parameters, i.e. the opening duration τ_λ of the electro-mechanical shutter SH, and the effective value $OD_{MES}(\lambda)$ of the optical density in the measurement arm. The range of the shutter's opening duration is between 40 ms (defined by its timing specification) and 1,000 s (chosen to ensure a reasonable duration for a single acquisition). Because of the large differences in the range of adjustment of this opening duration (1,000/0.04 = 25,000) and the transmittance change associated with a minimum OD_{MES} step (10 times), several sets of parameters $[\tau_\lambda, OD_{MES}]$ can often be used for the same level of transmission: in this case, the choice is always determined by the set corresponding to the smallest acquisition time.

Since the opening duration of the shutter is now fixed, we can only have the freedom to adjust the value $OD_{REF}(\lambda)$ of the optical density in the reference arm to achieve the same kind of locking for the maximum signal of the REF spectrum generated by the spatial dispersion of the light emitted from the end of the FOL2_R fiber. Depending on the discrete optical density sequence available in the reference arm (typical pitch of OD 0.3), the locking condition should nevertheless be relaxed to encompass a wider interval, i.e. between 25,000 and 57,500 in terms of maximum digitized signal.

Once the opening time of the shutter and the value of the optical densities in the measurement and reference arms have been defined, for each horizontal pixel of the CCD matrix, a summation of the digitized data corresponding to the vertical pixels 56 to 65 (respectively 190 to 199) is carried out to obtain the reference (respectively measurement) signal. The background levels associated with the reference (vertical pixels 1 to 5, and 126 to 130) and the measurement (vertical pixels 131 to 135, and 251 to 255) are similarly calculated. Finally, these background levels are subtracted from the related signals.

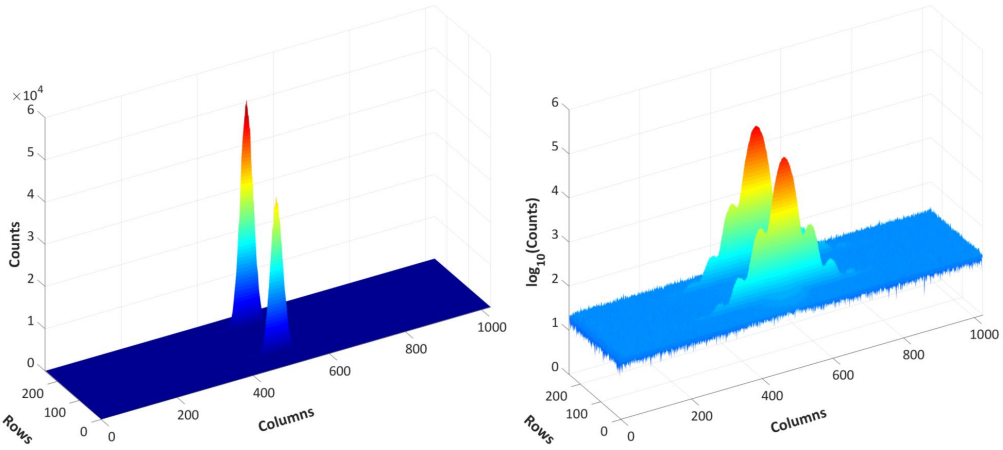

Fig. 2. Example of signal provided by the CCD matrix for a central wavelength of 600 nm (left graph, linear units; right, logarithmic units).

Figure 2 shows an example of the signal from the CCD matrix (1024 columns, 255 rows, 16

Optics EXPRESS

bits) when the LLTF and the spectrograph are tuned to a 600 nm wavelength; to the left in linear units, and to the right in logarithmic units. The MES spectrum corresponds to the rear peak whereas the REF spectrum corresponds to the front peak. Note the slight difference between the maximum levels of these two peaks and the high quality of the signal to noise ratio (the noise amplitude is approximately 5 counts for a maximum signal here of 55,000 counts).

2.3. Calibration and measurement

Thanks to the goniometric configuration of our set-up, a unique calibration procedure can be used for both transmittance and reflectance measurements, and is achieved, without sample and for $\theta = 180$ degrees, as follows: first, the reference signal is eliminated, by positioning the ODFWR filter wheel on slot 1 (the one containing a stop). This enables the set of parameters $[\tau_{\mathrm{BL}}(\lambda), \mathrm{OD}^{\mathrm{BL}}_{\mathrm{MES}}(\lambda)]$ associated with the baseline (BL) to be determined, i.e. to a 100% transmission in the measurement arm. Second, by sweeping through the various reference optical densities, that $[\mathrm{OD}^{\mathrm{BL}}_{\mathrm{REF}}(\lambda)]$ can be defined that satisfies the relaxed locking conditions introduced in the previous section. Let us call $S^{\mathrm{BL}}_{\mathrm{max}}(\lambda)$ the effective value of the maximum of the reference spectrum recorded under these conditions. When a filter transmittance or reflectance measurement is made, the first step is exactly the same and allows a new set of parameters $[\tau(\lambda), \mathrm{OD}_{\mathrm{MES}}(\lambda)]$ to be defined, but the tuning of the reference filter wheel is completely different: for each of the $k = 1$ to 20 optical density values accessible in the reference arm, the quantities

$$M(k,\lambda) = \tau(\lambda) \times 10^{-\mathrm{OD}_{\mathrm{REF}}(k,\lambda)} \frac{\mathrm{S}^{\mathrm{BL}}_{\mathrm{max}}(\lambda) - N_{\mathrm{BG}}}{\tau_{\mathrm{BL}}(\lambda) \times 10^{-\mathrm{OD}^{\mathrm{BL}}_{\mathrm{REF}}(\lambda)}} + N_{\mathrm{BG}} \tag{1}$$

are computed, where N_{BG} is the background noise of the CCD camera (typically 300); we choose the first k for which $M(k,\lambda)$ is less than 57,500. This choice ensures that the locking condition is automatically satisfied for the REF spectrum.

2.4. Data processing

Let us call $S_{\mathrm{MES}}(i,\lambda)$ [resp. $S_{\mathrm{REF}}(i,\lambda)$], the pre-processed measurement (resp. reference) spectrum (i.e. after vertical summation and background suppression) recorded by the CCD in the presence of the thin-film filter (where i is the pixel number), and $S^{\mathrm{BL}}_{\mathrm{MES}}(i,\lambda)$ [resp. $S^{\mathrm{BL}}_{\mathrm{REF}}(i,\lambda)$], the corresponding spectra recorded during the calibration.

For each set of variables (i,λ), first the local wavelength w is computed

$$w(i,\lambda) = \lambda + (i - 500)D \tag{2}$$

where D is the spatial dispersion of the spectrograph; then the local transmission t

$$t(i,\lambda) = \left[\frac{10^{-\mathrm{OD}_{\mathrm{MES}}} S_{\mathrm{MES}}(i,\lambda)}{10^{-\mathrm{OD}_{\mathrm{REF}}} S_{\mathrm{REF}}(i,\lambda)}\right] \times \left[\frac{10^{-\mathrm{OD}^{\mathrm{BL}}_{\mathrm{REF}}} S^{\mathrm{BL}}_{\mathrm{REF}}(i,\lambda)}{10^{-\mathrm{OD}^{\mathrm{BL}}_{\mathrm{MES}}} S^{\mathrm{BL}}_{\mathrm{MES}}(i,\lambda)}\right] \tag{3}$$

and finally the quality factor $Q(i,\lambda)$

$$\frac{4}{Q(i,\lambda)} = \frac{S_{\mathrm{HT}}}{S^{\mathrm{BL}}_{\mathrm{MES}}(i,\lambda)} + \frac{S_{\mathrm{HT}}}{S^{\mathrm{BL}}_{\mathrm{REF}}(i,\lambda)} + \frac{S_{\mathrm{HT}}}{S_{\mathrm{REF}}(i,\lambda)} + \frac{S_{\mathrm{LT}}}{S_{\mathrm{MES}}(i,\lambda)} \tag{4}$$

where S_{HT} (respectively S_{LT}) is a digital threshold applied to the incoming (respectively transmitted) light spectra. Relations (3) and (4) are only valid when all the $S(i,\lambda)$ are greater than the related thresholds; if not, they are replaced by

$$t(i,\lambda) = 0 \quad \text{and} \quad Q(i,\lambda) = 1 \tag{5}$$

Optics EXPRESS

The local wavelengths $w(i, \lambda)$ are then sorted in ascending order; this applies also to the local transmission and quality factor values. Then the spectral range $[\Lambda_{\min}, \Lambda_{\max}]$ of the transmittance measurement is defined as well as the wavelength pitch $\delta\Lambda$. For each wavelength Λ_k defined by

$$\Lambda_k = \Lambda_{\min} + (k-1)\,\delta\Lambda \tag{6}$$

all the local wavelengths $w(i, \lambda)$ that satisfy the condition

$$\Lambda_k - \frac{\delta\Lambda}{2} \leqslant w(i,\lambda) < \Lambda_k + \frac{\delta\Lambda}{2} \quad \forall i,\ \forall\lambda \tag{7}$$

are sought, and for all of them, the weighted transmittance $T(\Lambda_k)$ is computed:

$$T(\Lambda_k) = \frac{\sum Q(i,\lambda)\, t(i,\lambda)}{\sum Q(i,\lambda)} \tag{8}$$

In some cases, this weighted quantity might be equal to zero, which implies that the measurement of the transmittance of the thin-film filter is simply not possible in this specific spectral interval. The number of wavelengths Λ_k for which this situation occurs is designated N. Obviously, this number is a function of both digital thresholds S_{HT} and S_{LT}. The low threshold S_{LT} is defined from the electronic noise characterizing the spectra recording (typically 5 counts), while the high threshold S_{HT} is chosen to ensure a high signal to noise ratio for the reference and baseline measurements (typically better than 100).

3. Results and discussion

3.1. Band-pass filters

3.1.1. Qualification band-pass filter

To quantify the improvement in performance provided by the changes described in the previous sections, we first measured the spectral transmittance of the same filter as used during the first development phase of this spectrophotometric apparatus [19]. This is a band-pass filter consisting of 93 layers and manufactured by the Optical Thin-Film group of the Institut FRESNEL with a BÜHLER (BPF_IF) HELIOS deposition machine.

Figure 3 compares the spectral transmittance of this filter provided by both set-ups on the spectral range between 450 nm and 930 nm, while Fig. 4 shows the gain in terms of spectral resolution achieved between 682 nm and 692 nm. Note the remarkable coincidence between the transmittance spectra measured 2 years ago with SALSA 2 (the previous version of this set-up) and today with SALSA 3 (the new version described in this article), except around 687 nm, where the spectral resolution improvement (wavelength pitch 0.1 nm) allows a double transmission peak in a sharp transmittance resonance to be almost resolved. Recall that the corresponding transmittance levels are between 10^{-5} and 10^{-9}.

Finally, Fig. 5 gives two examples of spectra recorded by the CCD matrix used in the version of our set-up described in this paper. As recalled by the transmission graph inset at the left corner of this illustration, the filter is the same as that whose transmission measurement results are shown in Fig. 3. Two particular wavelengths were selected: first (yellow arrow), in the pass-band of the filter (λ = 782 nm), and second (green arrow), around the sharp resonance peak (λ = 680 nm) already presented in Fig. 4. Note that both REF and MES spectra are nearly identical in the first case (the spectral transmittance is flat around this wavelength), whereas the MES spectrum (red circles) is dramatically affected by the filter in the second case (the spectral transmittance changes very rapidly). It is even possible to recognize at the right side of the CCD signal (pixels 650-750), the rough shape of the nearly resolved resonance peak.

Optics EXPRESS

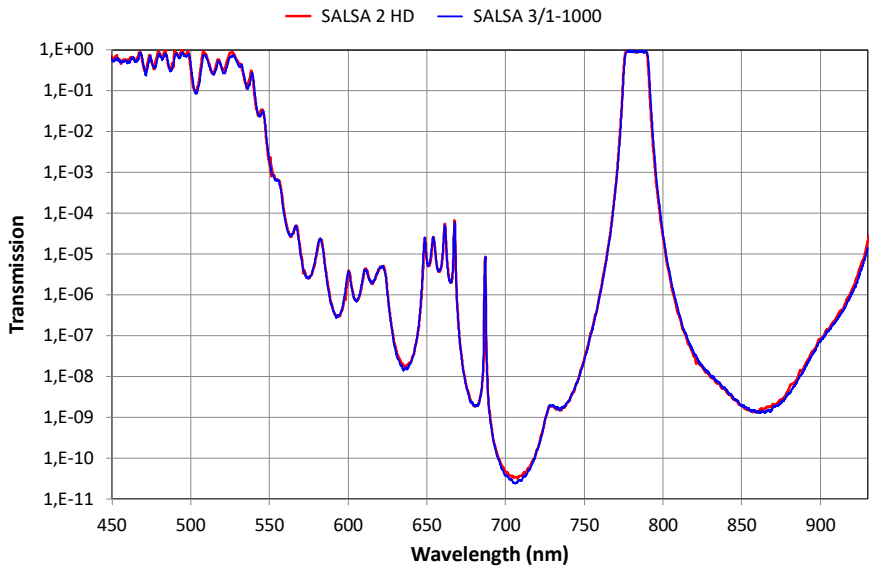

Fig. 3. Comparison of the spectral transmittance of a band-pass filter manufactured by the Institut FRESNEL (BPF_IF) and measured between 450 nm and 930 nm with the previous version of our set-up (SALSA 2, red line) and with the new version described in this article (SALSA 3, dark blue line).

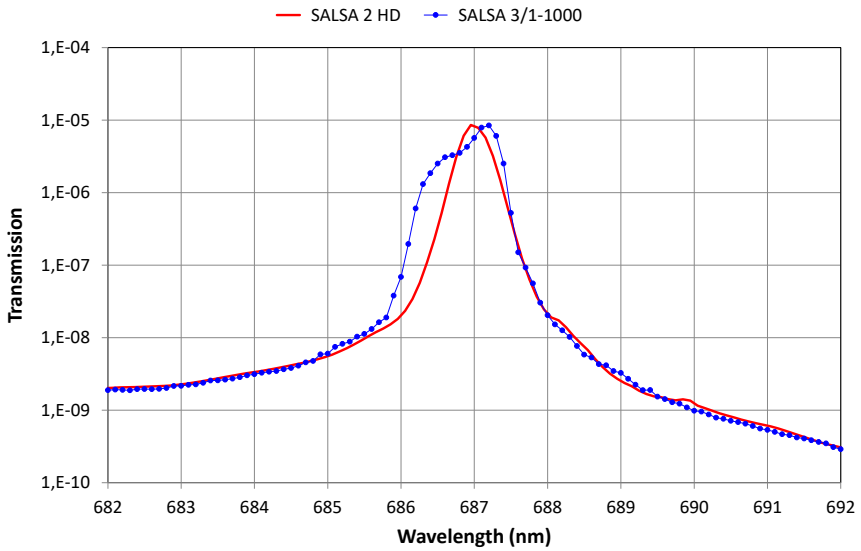

Fig. 4. Zoomed view of the spectral transmittance of the BPF_IF around a sharp transmission resonance centered at 687 nm, measured with SALSA 2 (red line) and with SALSA 3 (blue dots linked by blue line).

Optics EXPRESS

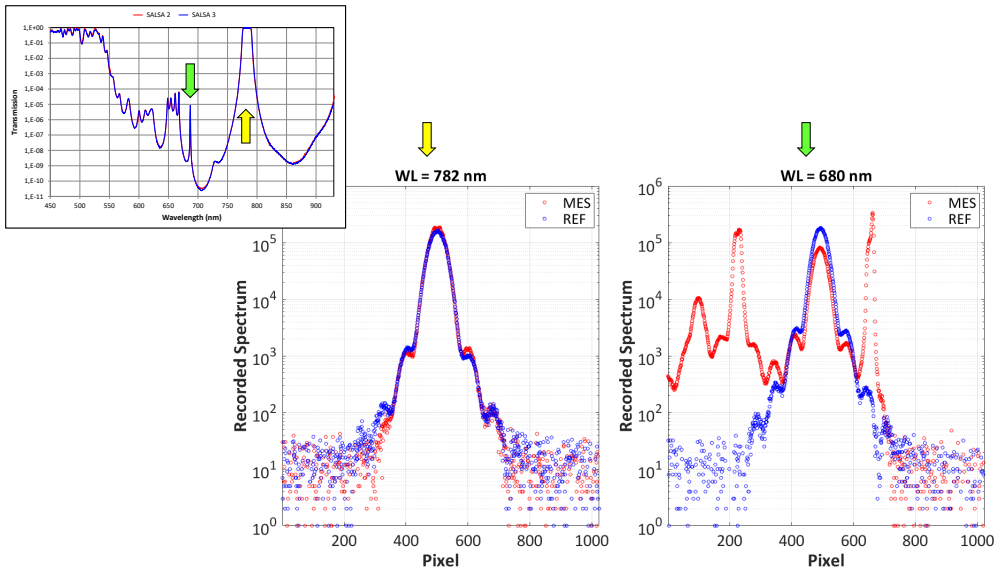

Fig. 5. Examples of recorded spectra at two different central wavelengths (680 and 782 nm).

3.1.2. High performance band-pass filter

To demonstrate the efficiency of this new version, we made the same kind of transmittance measurement on a high performance multiple cavity band-pass filter manufactured by VIAVI Solutions (BPF_VS), and characterized by very sharp band edges and high rejection levels. Figure 6 shows the transmittance spectrum of this filter measured with a wavelength pitch of 0.1 nm between 400 nm and 930 nm. The N number of missing data is here equal to 490 (instead of zero in the case of the BPF_IF filter), for an overall number of wavelengths of 5301. These missing data are essentially between 416 and 441 nm, 510 and 518 nm, and between 576 and 584 nm. Above a transmittance level of 2×10^{-10}, the agreement between experimental results and design data is impressive.

However, note that some discrepancies appear in the blocking regions on either side of the pass band, namely between 441 nm and 510 nm, and between 584 nm and 620 nm. Nevertheless, the corresponding signal to noise ratio (SNR) is clearly too high (between 10 and 1,000) to explain these discrepancies just by the influence of noise. A likely explanation of this phenomenon could be a parasitic contribution of the scattered light to such very low transmittance (the theoretical transmittance is around 10^{-22} at 460 nm and 10^{-18} at 650 nm). Indeed, as described in Section 2.1, the angular acceptance $\delta\theta_2$ of the receiving beam is defined by $\delta\theta_2 = a_2/f_2$, where $2a_2$ is the core diameter of the FOL2 fiber (100 μm) and f_2 the effective focal length (EFL) of the reflective collimator RRC (15 mm) used for reception. This leads to a total angular width $2\delta\theta_2$ of approximately 0.4 degree, which is obviously small, but probably enough to allow capture of a part of the light scattered around the direction of incidence by both faces of the filter (the filtering function is shared on the two faces of the substrate). Moreover, this effect is certainly amplified by the intrinsic divergence of the illuminating beam, that is half of that of the receiving beam (fiber core diameter $2a_1 = 50\,\mu$m, EFL $f_1 = 15$ mm).

A possible way of confirming this assumption is to drastically reduce the optical throughput of both beams, by replacing the multimode step index fibers used so far by two identical photonic crystal fibers (PCF) from NKT Photonics (Reference aeroGUIDE-8 [20]). Such fibers are indeed truly singlemode between 400 and 2,000 nm, and characterized by a modal field diameter (MFD)

Optics EXPRESS

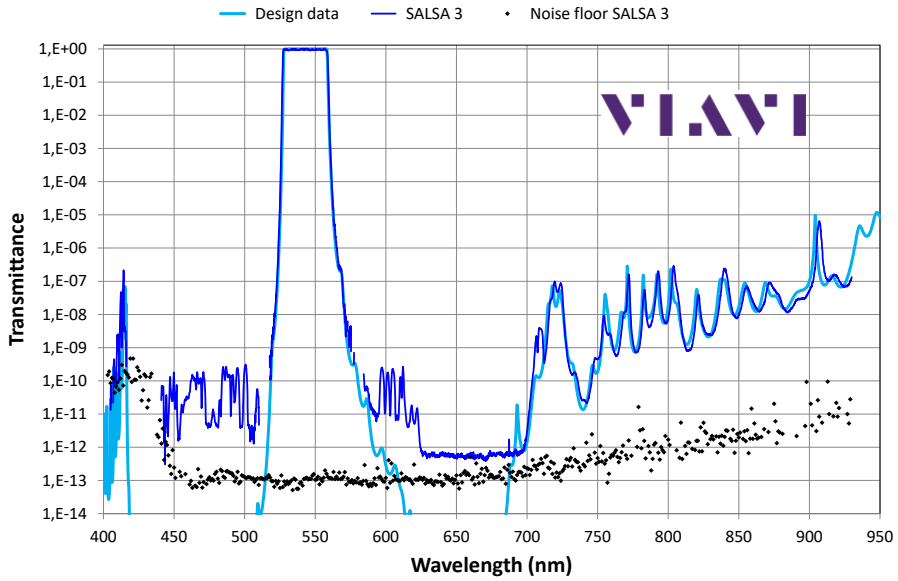

Fig. 6. Spectral transmittance measurement of a high performances band-pass filter manufactured by VIAVI Solutions (light blue continuous curve, design data; black diamond, measurement noise floor; dark blue line, data obtained with the set-up described in this paper).

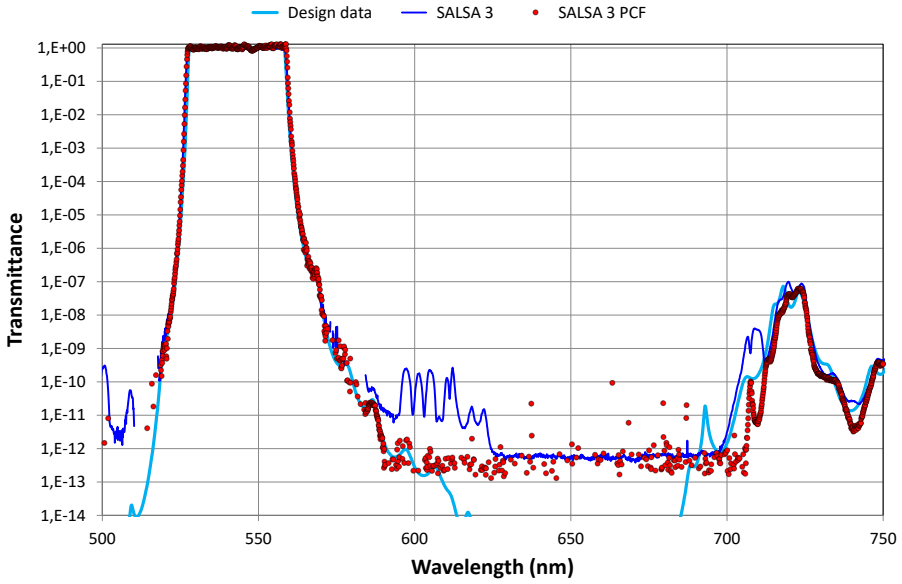

Fig. 7. Alternative spectral transmittance measurement of BPF_VS filter achieved with a modified version of SALSA 3 using PC fibers (light blue continuous curve, design data; dark blue line, data obtained with the nominal version of SALSA 3; red dots, data obtained with the PCF version of SALSA 3).

Optics EXPRESS

of 7.2 μm @ 532 nm: the corresponding detection solid angle is hence about 2×10^{-7} sr, which is nearly 200 times less than that of the standard receiving configuration. The only drawback of such a change is that the alignment tolerances become much tighter. Figure 7 shows the result of a transmittance measurement performed on BPF_VS filter with this modified set-up (red dots), compared to that achieved with the standard set-up (dark blue line).

We see that the questionable spectral pattern, recorded around 600 nm with the nominal version of SALSA 3, completely disappears, as expected. The price to pay for this improved angular selectivity is an increase in the noise floor (the coupling efficiency in the FOL1 fiber is significantly lower than that obtained for the standard multimode step index fiber). Consequently, this PCF configuration will be only implemented if needed.

3.2. Edge filters

The measurement of the steepness of edge and band-pass filters is key in the optical characterization of such components, because it defines their ability to reject intense laser lines whose central wavelength is very close to their pass-band. We will use here the definition of the steepness proposed by SEMROCK, namely the "actual distance between the place where OD>6 ends and the 50% transmission point" [21].

Figures 8 show zoomed views of the left and right edges of the pass-band of the VIAVI Solutions filter presented in the previous section. The steepnesses of the band edges of this filter are respectively 3.2 nm at the left (short wavelengths side) and 6.1 nm at the right (long wavelengths side), with, in both cases, a remarkable agreement between experimental measurements and design data. The set-up used for these measurements is the standard one (multimode step index fibers).

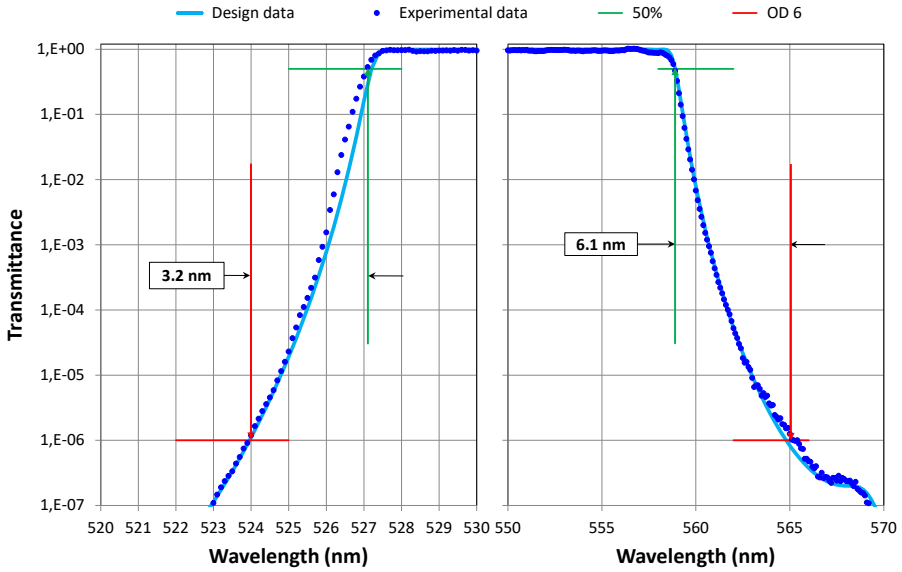

Fig. 8. Zoomed view of the edges of the pass band of the BPF_VS filter

In this case, the measurement dynamic range is mainly provided by adjustment of the optical densities during the spectral scanning of the band edge. However, when the filter steepness becomes smaller than the bandwidth of the illuminating beam, i.e. approximately 2 nm, the dynamic range cannot be obtained in this way and is entirely provided just by the intrinsic performance of the detection system.

Optics EXPRESS

Maximum signal recorded by a pixel of the CCD camera is typically 50,000, as indicated in section 2.1, while the vertical summation allows this level to be increased to 200,000, to be compared to the electronic noise (standard deviation approximately between 2 and 3 counts). So, to reach the dynamic range of 10^6 required to achieve a steepness measurement in accordance with SEMROCK's definition, we need to find a gain of approximately 5; this can be provided, for instance, by recording 25 independent spectra.

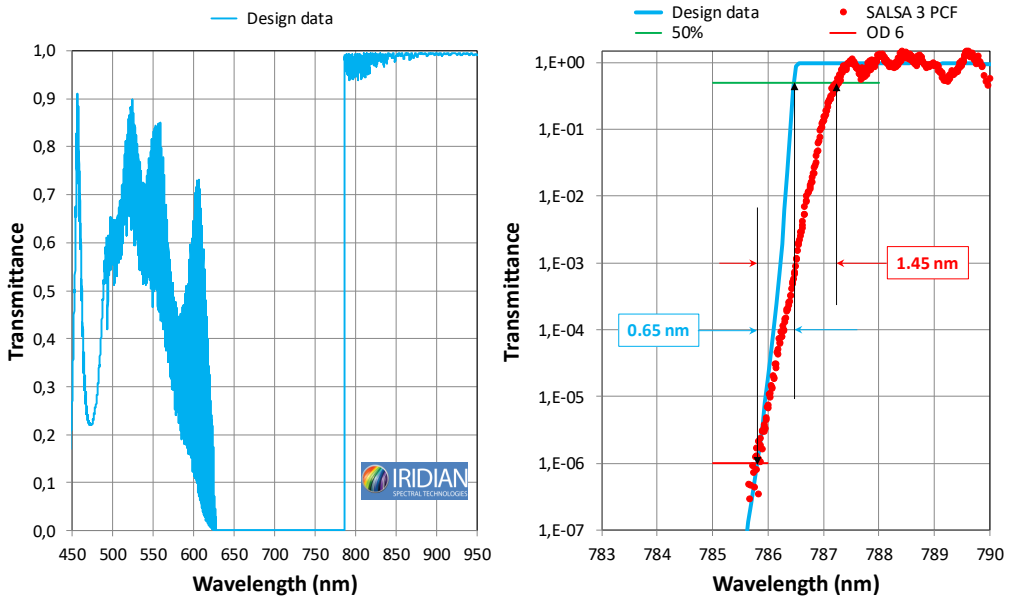

Fig. 9. Characterization of the steepness of a band edge filter manufactured by IRIDIAN Spectral Technologies (NanoEdge 785).

To confirm this rough estimate and demonstrate the ability of our set-up to properly characterize steepness below 2 nm, we characterized a NanoEdge 785 filter manufactured by IRIDIAN Spectral Technologies [22] whose theoretical steepness is 0.65 nm around 785 nm. To perform such a very narrow measurement, it is obviously essential to minimize the divergence of the illuminating beam: this is obtained by replacing the standard 50 μm core diameter multimode fiber by an aeroGUIDE-8 photonic crystal fiber. It is also necessary, as previously explained, to only use snapshot spectrum recordings, for three different central wavelengths (784.8 nm, 785.0 nm and 785.2 nm), and 16 recordings for each.

The result is shown in Fig. 9, and applying a basic quadratic deconvolution provides an estimate of the intrinsic performance of our system, namely a dynamic range of one million over only 1.3 nm.

3.3. *Silver layers*

To complete the demonstration of the performance of this new spectrophotometric bench, we measured the transmission of several silver layers deposited on 1 mm thick silica substrates, characterized by increasing thicknesses from 23 nm to 256 nm. The deposition apparatus used to manufacture these samples is the HELIOS machine from the Institut FRESNEL's Optical Thin Films Group. 4 identical silica substrates were installed in 4 different substrate holders: after 26.5 s of silver target sputtering under nominal conditions, a first substrate was extracted through the instrument's load-lock chamber. The second substrate was taken out after an overall deposition duration of 66.2 s, the third after 132.5 s and the last after 265 s.

Optics EXPRESS

The spectral transmission of these four different samples was measured with the nominal version of the SALSA bench described in this paper (i.e. using multimode fibers). The results are shown in Fig. 10 (colored dots). The thickness figures appearing at the right of the graph

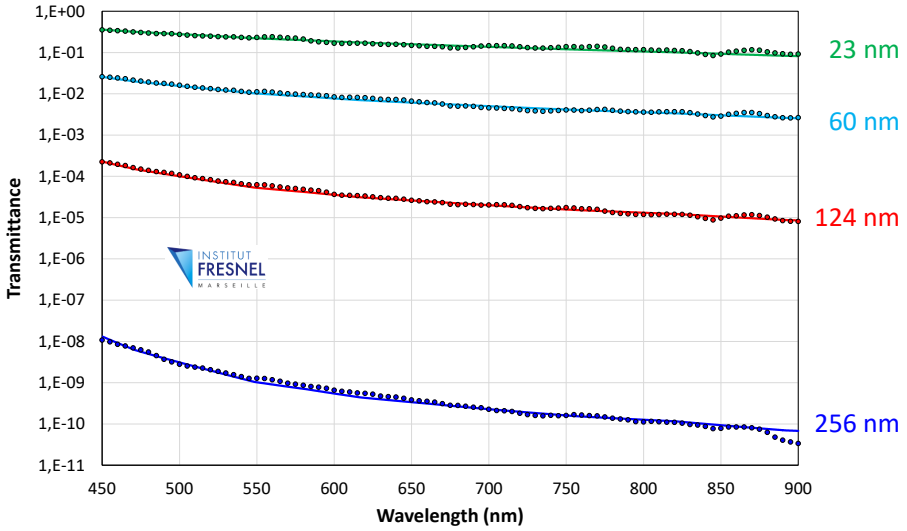

Fig. 10. Transmittance measurements of 4 different silver layers deposited on silica substrates with increasing thicknesses (colored dots, experimental results; colored continuous line, theoretical data).

are defined by minimizing the root-mean-square deviation between experimental results and theoretical data (colored continuous lines) computed using the silver refractive index data published by Johnson [23]. We observe the quality of the fit for all the thicknesses, despite the huge dynamic range of transmittance (close to 10^{10}). These results allow us to infer the silver deposition rate, namely 0.96 nm/s, and to highlight the perfect proportionality between each thickness and the corresponding deposition duration.

4. Conclusion and further achievements

In this paper, we described an upgraded version of a spectrophotometric bench developed at the Institut FRESNEL from 2014 [19] that enables determination of the spectral transmission of high performance interference filters with simultaneously huge dynamic range (the noise floor is close to 10^{-13}) and high spectral resolution (approximately 0.1 nm). This breakthrough instrument provides a 6 orders of magnitude improvement in transmission measurements with respect to the best commercially available spectrophotometers (PERKIN-ELMER Lambda 1050 or AGILENT Cary 7000) and more than 4 orders of magnitude with respect to the new HELIX spectrophotometric apparatus recently developed by the thin-film company ALLUXA [24].

Moreover, the structure of this bench allows also optical filters to be characterized by angle and wavelength resolved measurements of their scattering properties [25] over the same spectral range (from 400 nm up to 930 nm).

Further improvements will be devoted to the implementation of rotating polarizers, both into illuminating and receiving beams, as well as extending the detection range towards short-wave infrared up to 1.7 μm.

Optics EXPRESS

Funding

Centre National d'Etudes Spatiales (CNES); Direction Générale de l'Armement (DGA).

Acknowledgments

The authors greatly appreciated fruitful exchanges with Markus Tilsch at VIAVI Solutions, as well as Brian Sullivan at IRIDIAN Spectra Technologies Ltd, and would like to thank the Optical Thin-Film group of the Institut FRESNEL, especially Thomas Begou and Julien Lumeau, for the manufacture of the qualification band-pass filter and the deposition of the silver layer trial samples.

References

1. A. V. Tikhonravov, M. K. Trubetskov, and G. W. DeBell, "Application of the needle optimization technique to the design of optical coatings," Appl. Opt. **35**, 5493–5508 (1996).
2. see for instance http://www.optilayer.com/
3. S. W. Anzengruber, E. Klann, R. Ramlau, and D. Tonova, "Numerical methods for the design of gradient-index optical coatings," Appl. Opt. **51**, 8277–8295 (2012).
4. F. Lemarchand, "Application of clustering global optimization to thin film design problems," Opt. Express **22**, 5166–5176 (2014).
5. R. Götzelmann, A. Zöller, W. Klug, K. Matl, and H. Hagedorn, "Plasma Ion Assisted Deposition: An Innovative Technology for High Quality Optical Coatings," Proceedings of the 40th annual technical conference, Society of Vacuum Coaters, 320–326 (1997).
6. R. Sargent, M. Tilsch, G. Ockenfuss, K. Hendrix, M. Grigonis, and A. Bergeron, "Advances in precision optical coatings through the use of a fast-cycle sputter coater," Proceedings of the 51st annual technical conference, Society of Vacuum Coaters (2008).
7. M. Scherer, J. Pistner, and W. Lehnert, "UV- and VIS Filter Coatings by Plasma Assisted Reactive Magnetron Sputtering (PARMS)," in *Optical Interference Coatings*, OSA Technical Digest (Optical Society of America, 2010), paper MA7.
8. T Begou, H. Krol, D. Stojcevski, F. Lemarchand, M. Lequime, C. Grezes-Besset, and J. Lumeau, "Complex optical interference filters with stress compensation for space applications," CEAS Space J. **9**, 441–449 (2017).
9. K. D. Hendrix, C. A. Hulse, G. J. Ockenfuss, and R. B. Sargent, "Demonstration of narrowband notch and multi-notch filters," Proc. SPIE **7067**, in *Advances in Thin-Film Coatings for Optical Applications V*, 706702 (2008);
10. K. Hendrix, "Linear variable filters for NASA's OVIRS instrument: pushing the envelope of blocking," Appl. Opt. **56**, C201-C205 (2017).
11. R. Le Goff, B. Badoil, P. Fuss, F. Tanguy, and P. Etcheto, "Recent developments of multispectral filter assemblies for CCD, CMOS and bolometer," Proc. SPIE **8176**, in *Sensors, Systems, and Next-Generation Satellites XV*, 817618 (2011).
12. R. Le Goff, H. Krol, M. Lequime, B. Badoil, G. Montay, and K. Gasc, "Multispectral Filters Assemblies for Earth Remote Sensing Imagers," International Conference on Space Optics ICSO, Tenerife (2014).
13. G. J. Ockenfuss, N. A. O'Brien, and E. Williams, "Ultra-low stress coating process: an enabling technology for extreme performance thin film interference filters," Optical Fiber Communication Conference and Exhibit, Anaheim, CA, 2002, paper FA8.
14. M. K. Tilsch, R. B. Sargent, and C. A. Hulse, "Dielectric Multilayer Filters," in *Wavelength Filters in Fibre Optics*, Springer Series in Optical Sciences **123**, H. Venghaus, ed. (Springer, 2006).
15. J. W. Lichtman and J. A. Conchello, "Fluorescence microscopy," Nat. Methods **2**, 910–919 (2005).
16. L. Pinard, C. Michel, B. Sassolas, L. Balzarini, J. Degallaix, V. Dolique, R. Flaminio, D. Forest, M. Granata, B. Lagrange, N. Straniero, J. Teillon, and G. Cagnoli, "Mirrors used in the LIGO interferometers for first detection of gravitational waves," Appl. Opt. **56**, C11–C15 (2017).
17. D. Vander-Hyde, C. Amra, M. Lequime, F. Magana-Sandoval, J. R. Smith, and M. Zerrad, "Optical scatter of quantum noise filter cavity optics," Class. Quantum Gravity **32**, 135019 (2015).
18. S. Liukaityte, M. Lequime, M. Zerrad, T. Begou, and C. Amra, "Broadband spectral transmittance measurements of complex thin-film filters with optical densities of up to 12," Opt. Lett. **40**, 3225–3228 (2015).
19. M. Lequime, S. Liukaityte, M. Zerrad, and C. Amra, "Ultra-wide-range measurements of thin-film filter optical density over the visible and near-infrared spectrum," Opt. Express **23**, 26863–26878 (2015).
20. https://www.nktphotonics.com/wp-content/uploads/sites/3/2015/03/aeroGUIDE.pdf?1539608269.
21. https://www.semrock.com/transition-width-edge-steepness.aspx.
22. https://www.iridian.ca/product/785-nano-edge/.
23. P. B. Johnson and R. W. Christy, "Optical constants of the Noble Metals," Phys. Rev. B **6**, 4370 (1972).
24. A. Johansen, A. Czajkowski, N. Cooper, M. Scobey, P. Egerton, and R. Fortenberry, "A new spectral analysis system designed to measure high-performance optical filters," Alluxa White Paper Series (2017).

Optics EXPRESS

25. M. Zerrad, M. Lequime, S. Liukaityte, C. Amra, "Parasitic light scattered by complex optical coatings: Modelization and metrology," CEAS Space J. **9**, 473–484 (2017).